

Supporting Information

Stomata-like Metal Peptide Coordination Polymer

Ning Ma,^{a†} Cong Lin,^{b†} Nian Wu,^c Qi Liu,^a Jia-Le Ma,^d Wei Meng,^e Xiao-Shuang Wang,^a Lu Zhang,^a Xiaohui Xu,^a Yifang Zhao,^b Lin Zhuang,^c Jun Fan,^d Junliang Sun,^{b*} Ren-Xi Zhuo,^a and Xian-Zheng Zhang^{a*}

^a Key Laboratory of Biomedical Polymers of Ministry of Education, The Institute for Advanced Studies & Department of Chemistry, Wuhan University, Wuhan 430072, P. R. China.

^b College of Chemistry and Molecular Engineering, Peking University, Beijing 100871, P. R. China.

^c Department of Chemistry, Hubei Key Lab of Electrochemical Power Sources, Wuhan University, Wuhan 430072, P. R. China,

^d Department of Physics and Materials Science, City University of Hong Kong, Hong Kong SAR, P. R. China.

^e Department of Materials Science and Engineering, College of Engineering, Peking University, Beijing 100871, P. R. China.

E-mail: xz-zhang@whu.edu.cn (X.-Z. Zhang); junliang.sun@pku.edu.cn (J. Sun).

† N. M. and C. L. contributed equally.

1. Experimental Procedures

Synthesis of Gly-Thr: Gly-Thr was manually synthesized in 1.01 mmol scale on the 2-chlorotrityl chloride resin, employing a standard Fmoc chemistry by solid phase peptide synthesis (SPPS) method. The coupling of the first residue used 3 equiv of Fmoc-protected amino acid (Fmoc-Thr-OH) relative to resin substitution degree with 6 equiv of DIEA in a DMF solution. Fmoc-Gly-OH was carried out with 4 equiv of Fmoc-protecting amino acid, 6 equiv of DIEA and 4 equiv of HBTU and Hobt for 4 h. During the synthesis, the Fmoc protecting groups were deprotected with 20 % (v/v) piperidine/DMF twice. The cleavage of peptide was performed in a mixture of deionized water, TIS and TFA in the ratio of 2.5:2.5:95. After 2 h stirring at room temperature, the mixture was collected. The excess TFA was removed by rotary evaporation and the remaining viscous peptide solution was precipitated in the cold ether. The resulting product was collected and freeze-dried. ESI-MS (H₂O): 175 [M - H].

Synthesis of Powder Crystals: Cu-(Gly-Thr)•2H₂O (CuGT; Gly-Thr = C₆H₁₂N₂O₄) was prepared as the following typical experiment. 11 mg (0.0625 mmol) of Gly-Thr and 8 mg (0.0331 mmol) of Cu(NO₃)₂•2H₂O were transferred to a 4 mL rubber-lined capped scintillation vial containing 3 mL of methanol. The mixture was sonicated for 10 minutes, followed by addition of 80 µL 1M NaOH (aq). Next, the blue methanolic solution was shaken on (ZHWY-1102C) shaking table at 300 rpm per minute for 20 minutes, giving rise to the formation of blue crystals suitable for X-ray crystallography (63% yield). The crystalline product was then filtered from the reaction mixture, thoroughly washed with CH₃OH and sealed. This formula is confirmed by thermogravimetric analysis (see below), suggesting the compositional formula of **1** is Cu-(Gly-Thr)•2H₂O. The CHN and the inductive coupled plasma (ICP) analysis of the bulk material indicates a formula of [Cu(Gly-Thr)]•(H₂O)₂. Despite this small variation in solvent content between the analysed singlecrystal and the bulk sample, analytical data of the desolvated (bulk) sample clearly shows the framework has a formula of Cu(Gly-Thr).

Bulk microanalytical and ICP (Cu) data for Cu-(Gly-Thr)•2H₂O:

Measured: C = 26.50%; H = 4.72%; N = 10.35%; Cu = 23.20%

Calculated: C = 26.33%; H = 5.16%; N = 10.23%; Cu = 23.21%

Bulk microanalytical and ICP (Cu) data for desolvated Cu-(Gly-Thr):

Measured: C = 29.92%; H = 4.27%; N = 11.72%; Cu = 26.37%

Calculated: C = 30.32%; H = 4.24%; N = 11.79%; Cu = 26.73%

Synthesis of Single Crystals: 5 mg powder crystalline product was dissolved adequately in 0.45 ml ultrapure water, and then the homogeneous system was placed in tranquil surroundings, and exposed to the air at room temperature. Sheet-shape blue crystal was crystallized out after 120 hours.

Scanning Electron Microscopy (SEM) and Transmission Electron Microscopy (TEM): SEM and TEM were carried out by FEI-QUANTA 200 and JEM-2100 HR, respectively.

Element distribution: Element distribution was obtained using JEOL JSM 6510LV scanning electron microscope (SEM, Hitachi, Japan) and EMAX EX-450 Energy dispersive X-ray fluorescence spectrometer (EDX).

Sample handling: On storing, if as-made solid is dried and stored as a dry powder on the bench or in a refrigerator, the structure transforms into wet phase (as evidenced by powder X-ray diffraction (PXRD) measurements) within 2 days. The structure of as-made solid remains unchanged if it is stored in the CH₃OH or under an inert atmosphere such as in a glovebox.

Powder X-ray Diffraction: For **1**, powder X-ray diffraction data were collected in transmission geometry using a Rigaku Smartlab (9 kW) XG diffractometer with Cu K α ₁ ($\lambda=1.5406$ Å) radiation. For **1a**, powder X-ray diffraction data were collected in transmission mode using a capillary spinner on PNAlytical Empyrean diffractometer with Cu K α radiation. For **1b**, powder X-ray diffraction data were collected in transmission mode using a Bruker D8 Advance diffractometer with high-low temperature modules. PXRD pattern in different humidity were collected on a Bruker Advance D8 diffractometer (Cu K α radiation, $\lambda=1.5418$ Å) with homemade humidity control equipment. The sample was loaded in the equipment and fixed at 0%, 25%, 75% and 98% during testing.

In situ variable temperature powder X-ray diffraction experiments were carried out on a Bruker Advance D8 diffractometer (Cu K α radiation, $\lambda=1.5418$ Å) with a computer-controlled furnace. The sample was pretreated by soaked in RH 100% water vapor for 3 days. The sample was loaded on a platinum strip and heated from 25 °C to 235 °C at a heating rate of 5 °C/min, and the PXRD data were collected after the temperature was stabilized for 5 min at every chosen temperature.

Single Crystal X-ray Diffraction: Single crystal of **1** was isolated directly from the reaction vessel. A sample of crystals and mother liquor were extracted, placed under paratone/fomblin Y-1800 on a microscope slide and a candidate blue crystal was isolated and mounted to a Mitegen tip. The mounted sample was immediately placed on an AXS APEX DUO goniometer. Data was collected using a Saturn 724+ detector and 007HF Molybdenum micro-focus rotating anode X-ray source. Single crystal X-ray diffraction measurements of **1a** was performed using a boron glass capillary spinner on X-ray diffractometer with graphite monochromator and Mo K α radiation. The structures were solved using direct methods and expanded using Fourier techniques. The refinements were carried out using full-matrix least squares techniques on F^2 using SHELXL-2014 and OLEX2 (Table S1).^{S1-3} [CCDC 1487469 and 1487560 contain the supplementary crystallographic data for this paper. These data can be obtained free of charge from The Cambridge Crystallographic Data Centre via www.ccdc.cam.ac.uk/data_request/cif.]

Thermal Gravimetric Analysis (TGA) and Thermal Gravimetric-mass spectrometric (TG-MS) Analysis: TGA was performed on a TGS-2 thermogravimetric analyzer (Perkin-Elmer). TG-MS was carried out by STA449C/Qms 403C.

Differential Scanning Calorimetry (DSC): DSC was carried out on a Q-2000 Instrument (TA).

Fourier Transform-Infrared Spectroscopy (FT-IR): The samples in KBr pellets were analyzed by FT-IR spectrophotometer (Perkin-Elmer Spectrum 100) and Spectrum 400 instruments equipped for conducting high temperature transmission infrared spectroscopy. The transmission experiments were carried out by polished 25 mm \times 5 mm KBr discs. Thirty-two scans were loaded in order to achieve an acceptable single-to-noise ratio. In all case, spectral resolution was maintained at 4 cm⁻¹. The sample assembly was then placed in a heating stage and heated at a rate of 10 °C/min using a Watlow SD6C-HCAA-AARG temperature controller. The infrared scans were obtained every 10 seconds to assure that uniform temperature is achieved. Since **1** is solid at room temperature, attenuated total reflection (ATR) was conducted on **1** using a Perkin Elmer FTIR Spectrum 100 together with a universal ATR sampling accessory. A diamond crystal was used as the reflectance unit and pressure was applied on the samples using a pressure arm.

¹H Nuclear Magnetic Resonance (¹H NMR): ¹H NMR spectra were recorded on a Mercury VX-300 spectrometer (Varian) at 300 MHz by using D₂O as the solvent.

Computational Method: Periodic crystal systems were investigated by spin polarized density functional theory (DFT) within the Perdew-Burke-Ernzerhof generalized gradient approximation (GGA-PBE),⁵⁴⁻⁷ as implemented in the Vienna ab initio Simulation Package (VASP 5.3).^{58,9} The electron-ion interactions were described by projected augmented wave (PAW)^{510,11} methods with a kinetic energy cutoff of 420 eV. Electrons on states of (3p, 3d and 4s) of Cu, (1s) of H, (2s, 2p) of C, N and O are taken as valence electron. To correctly depict interaction caused by polarization and dispersion, van der Waals (vdW) interactions was included by Density Functional Theory Tkatchenko-Scheffler (DFT-TS) method.

The initial primitive cell structures at wet and dry states came from the results of single crystal diffraction. After the optimization by DFT, the lattice parameters of **1** were $a = 4.761 \text{ \AA}$, $b = 8.355 \text{ \AA}$, $c = 22.067 \text{ \AA}$, $\alpha = 90^\circ$, $\beta = 102.58^\circ$ and $\gamma = 90^\circ$ (experimental data: $a = 5.22 \text{ \AA}$, $b = 8.635 \text{ \AA}$, $c = 23.116 \text{ \AA}$, $\alpha = 90^\circ$, $\beta = 100.1^\circ$ and $\gamma = 90^\circ$). In the meantime, the optimized lattice parameters of **1a** were $a = 5.053 \text{ \AA}$, $b = 8.514 \text{ \AA}$, $c = 17.041 \text{ \AA}$, $\alpha = 90^\circ$, $\beta = 90^\circ$ and $\gamma = 90^\circ$ (experimental data: $a = 5.28 \text{ \AA}$, $b = 8.718 \text{ \AA}$, $c = 17.773 \text{ \AA}$, $\alpha = 90^\circ$, $\beta = 90^\circ$ and $\gamma = 90^\circ$).

During the geometry optimization, all of the atoms were relaxed using a conjugate gradient method until the Hellmann-Feynman force on every atom could be smaller than 0.01 eV/\AA . In addition, the total energy converged to $1e^{-5} \text{ eV}$ and the Brillouin zone was sampled with a $4 \times 2 \times 1$ Monkhorst-Pack k point grid.⁵¹⁰ The method of Gaussian smearing was applied with a smearing width of 0.1 eV to determine how the partial occupancies.

The charge density difference ($\nabla\rho$), for the wet state, was obtained between the charge density of the total system (i.e. that of the whole structure of the optimized wet state) and the isolated subsystems. For the case of a peptide aggregate with the coordinated Cu atoms (Cu-GT/H₂O system), the argument of the integral is $\nabla\rho(\text{Cu}) = \rho[\text{Cu/GT/H}_2\text{O}] - \rho[\text{GT/H}_2\text{O}] - \rho[\text{Cu}]$. While for the H₂O-Cu/GT system, the argument of the integral is $\nabla\rho(\text{H}_2\text{O}) = \rho[\text{Cu/GT/H}_2\text{O}] - \rho[\text{Cu/GT}] - \rho[\text{H}_2\text{O}]$.

The Perdew-Wang 91 Generalized Gradient Approximation⁵¹¹ within the DFT formalism⁵¹² was used in this study as provided by the module DMol³ in Materials Studio software developed by Accelrys Inc..^{513,14} All geometry optimization calculations were performed using the double numerical with polarization (DNP) basis set, including spin polarization and dispersion effect with OBS method. The self-consistent field procedure converges until the energy difference was smaller than $1e^{-5} \text{ eV}$ and the Hellmann-Feynman force was smaller than 0.054 eV/\AA . The real-space global orbital cutoff radius was set to be 4.4 \AA . The fractional occupation was determined through smearing electrons by an energy width of 0.5 eV near the Fermi level.

The single point energy of each frame was performed to explore the minimum energy reaction path and energy barrier to conquer for the transformation. To compromise computational cost and accuracy, we abstract a cluster of non-periodic models with a single copper cation and the related molecular fragments under water layer or not, to simulate the process we have inferred from experimental and theoretical results. To obtain a theoretical stable geometry, we extract models from the original periodic structures (**1** and **1a**) as initial and final geometry. Details of the models were exhibited in **Fig. 3d**. Through interpolating 7 intermediate images between initial state and final state, simulating calculations displayed the rotation and bond-breaking/reforming process.

Gas Adsorption Analysis: Static CO₂ (-78°C) adsorption of the sample were measured by Autosorb-iQ gas sorption system (Quantachrome).

Dynamic Adsorption Analysis: Breakthrough experiments were performed on a $0.5 \text{ cm} \times 5.0 \text{ cm}$ stainless steel Swagelok bed with adsorbent inside. The sample was heated for regeneration by using a Thyristor control cabinet with heating mantle at 80°C for 30 minutes. The flow rate of the gases was determined at 10 mL/min by D08-1F digital mass flow controllers. The wet state was obtained by pumping in humidified helium to the sample bed for 2 hours. The relative humidity of the flowing gas was 34%. The temperature of the water bath was controlled at 25°C . The gaseous effluent from the sample bed was

monitored for CO₂ by using a Stanford Research Systems QMS200 Gas Analyzer mass spectrometer. The breakthrough time was calculated by the equation below:

$$\tau = \frac{(t - t_0) * v}{L * \alpha} \quad (1)$$

Where t and t_0 are the measured breakthrough time of the material and empty bed, respectively; v is flow velocity (volume flow / cross-sectional area); L is the length of adsorbent bed and α is filling factor.

2. Crystal Structures and morphology of **1** and **1a**

Table S1. Crystallographic data

CCDC number	1487469	1487560
Empirical formula	C ₆ H ₁₀ CuN ₂ O ₄ ·2(H ₂ O) (1)	C ₆ H ₁₀ CuN ₂ O ₄ (1a)
Formula weight	273.74	237.70
Temperature /K	296	180
Crystal system	Monoclinic	Orthorhombic
Space group	<i>P</i> 2 ₁	<i>P</i> 2 ₁ 2 ₁ 2 ₁
a/ Å	5.222(2)	5.287
b/ Å	8.635(4)	8.718
c/ Å	11.558(5)	17.773
α/°	90.00	90.00
β/°	100.115	90.00
γ/°	90.00	90.00
Volume/ Å³	513.1	819.1
Z	2	4
ρ_{calc} mg/mm³	1.772	1.928
m/mm⁻¹	2.141	2.649
F(000)	282	484
Crystal size/mm³	0.220×0.100×0.005	0.30×0.20×0.05
Θ range for data collection	2.96 to 28.59°	4.02 to 26.01°
Index ranges	-7≤h≤7, -11≤k≤10, -15≤l≤15	-6≤h≤4, -8≤k≤10, -14≤l≤21
Reflections collected	2257	1500
Independent reflections	2018	1138
Refinement method	SHELXL-97	SHELXL-97
Data/restraints/parameters	2257/3/133	1500/8/79
Goodness-of-fit on F²	1.032	1.067
Final R indexes [I>2σ(I)]	R ₁ =0.0474, wR ₂ =0.1128	R ₁ =0.1119, wR ₂ =0.2700
Final R indexes [all data]	R ₁ =0.0533, wR ₂ =0.1167	R ₁ =0.1317, wR ₂ =0.2811
Largest diff. peak/hole/e Å⁻³	0.0491/-0.496	2.564/-1.878

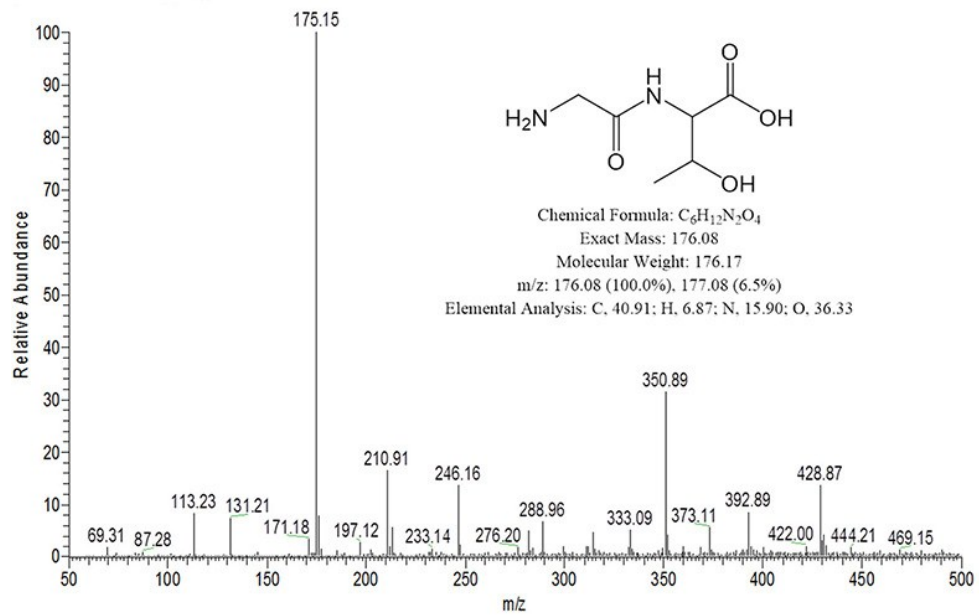


Fig. S1 Mass spectrum of GT.

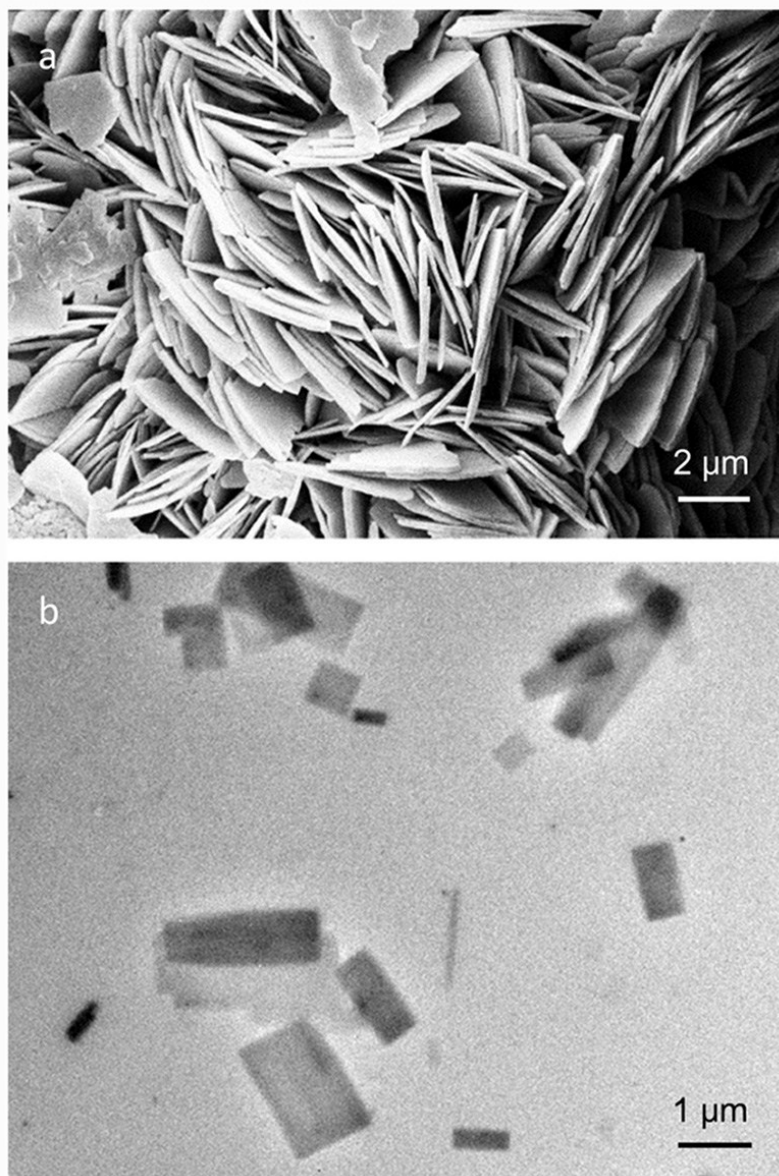


Fig. S2 SEM and TEM image of powder crystals. a) SEM image of crystals with uniform size and regular plate morphology. b) TEM image of powder crystals.

SEM and TEM images of as-made **1** show the formation of microcrystalline PCPs with monoclinic flake morphology.

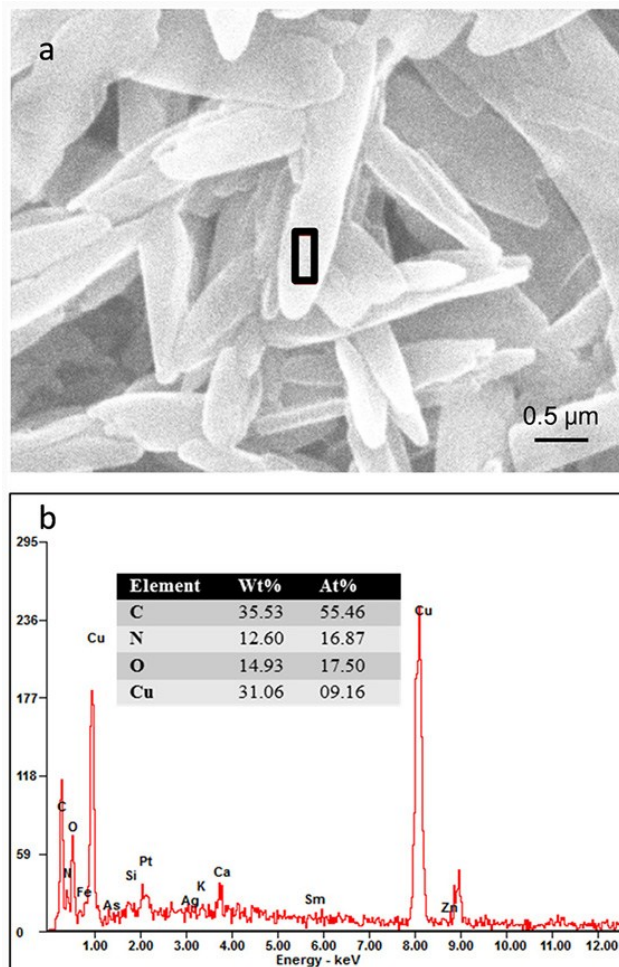


Fig. S3 a) SEM and b) EDX of the selected area in the a) of the powder crystal.

Element distribution of **1** shows that molar ratio of Cu to C 1:6 and Cu to N 1:2, indicating the molar ratio of Cu to Gly-Thr is 1:1.

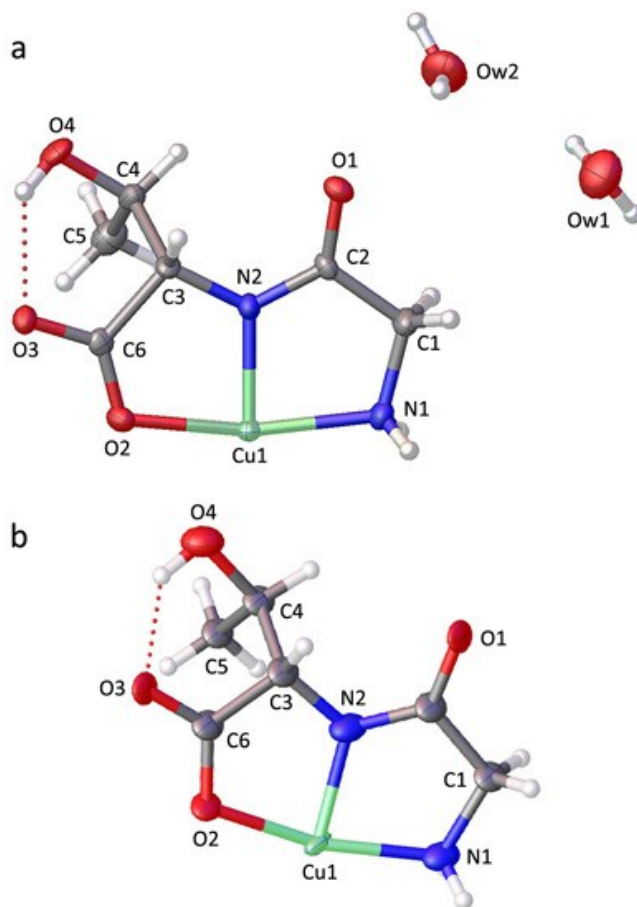


Fig. S4 Ortep representation of the asymmetric unit in a) [Cu-(Gly-Thr)]•2H₂O (**1**) and b) Cu-(Gly-Thr) (**1a**). H-bond (dashed line) between the -OH group from the threonine side chain and the terminal carboxylate group (O4H4A•••O3, 2.037(2)).

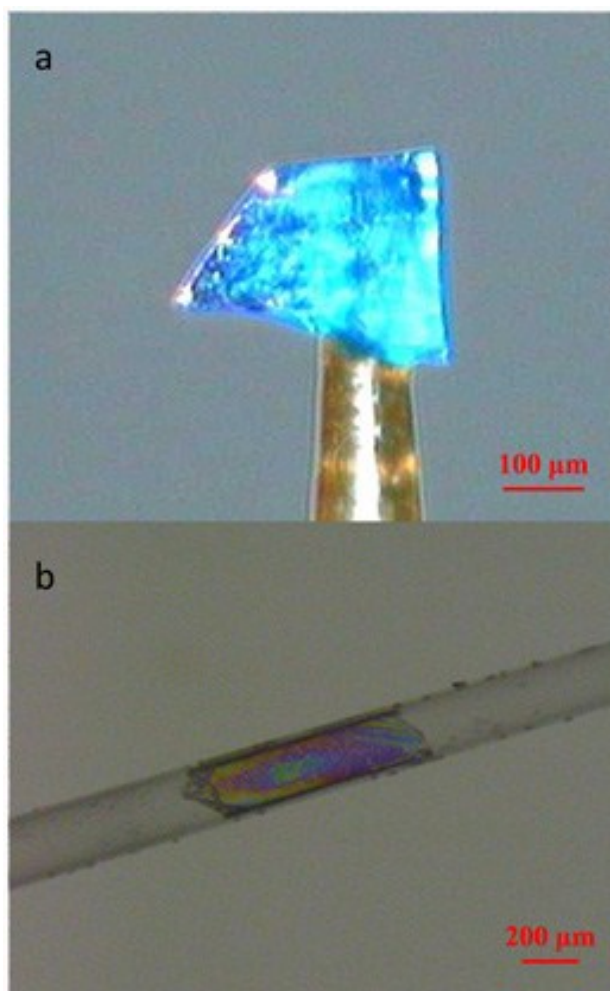


Fig. S5 Pictures of the single crystal of **1** (a) and **1a** (b) showing its color, size and morphology.

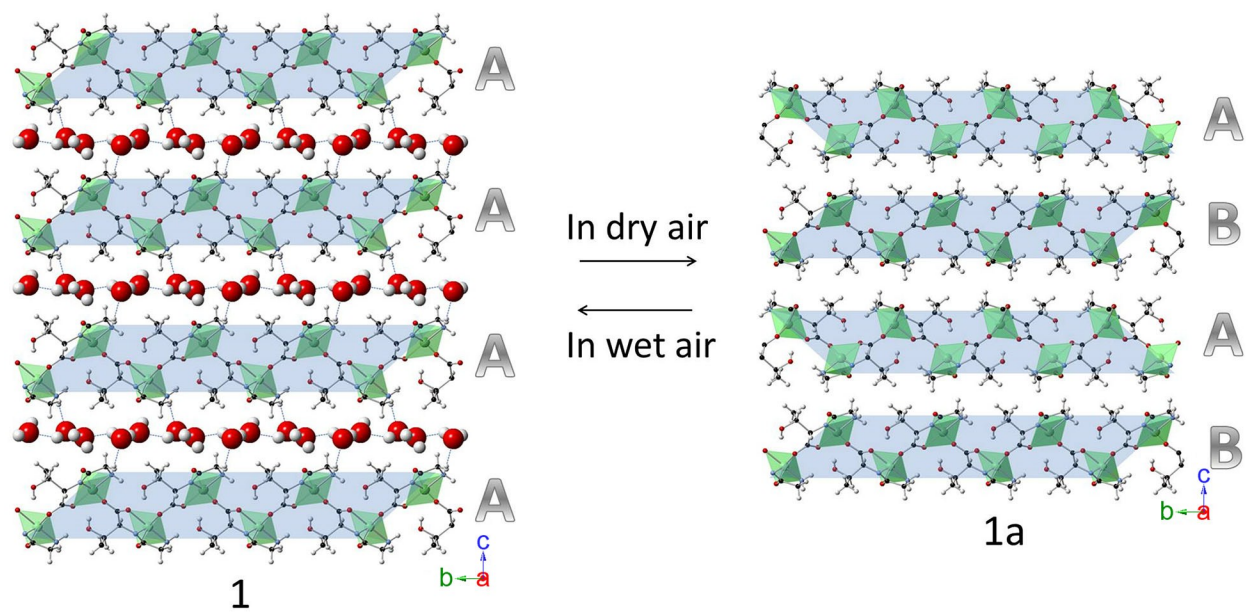


Fig. S6 Schematic diagram of structure transformations.

3. Thermoanalysis and Stability Analysis of **1**

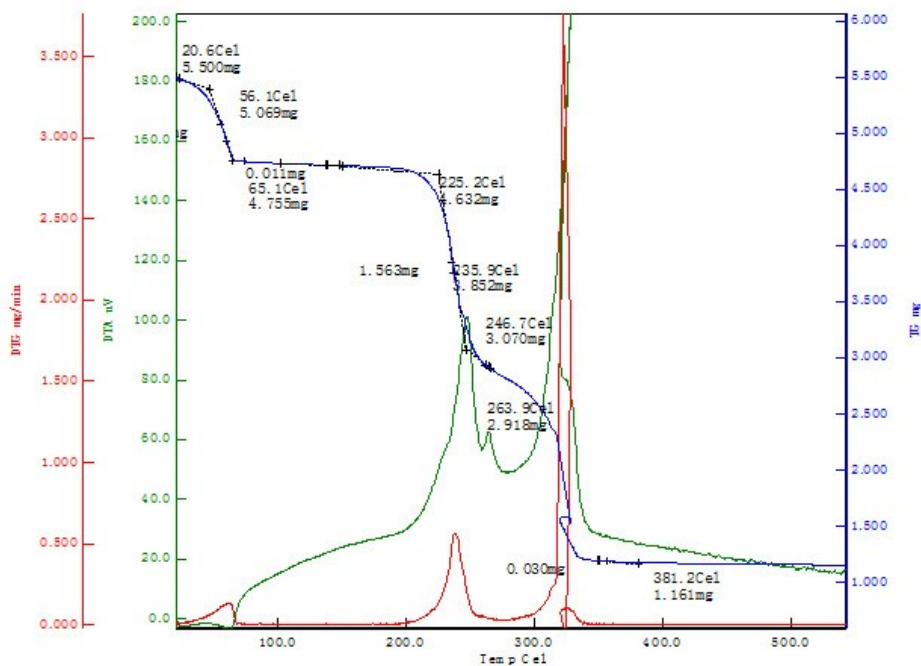


Fig. S7 TG, DTG and DTA curves of **1**.

The stepwise thermogravimetric curve of **1** in air indicates that the release of the guest water molecules, which was measured 13.5 wt% loss (calculated 13.2 wt%), occurred at 50 °C to give the dehydrated form (**1b**), which is stable up to 235 °C. Therefore, **1b** can be accomplished by heating at the temperature range between 50 and 235 °C. On further heating, GT molecules are decomposed at 237 °C, forming an unidentified brown amorphous.

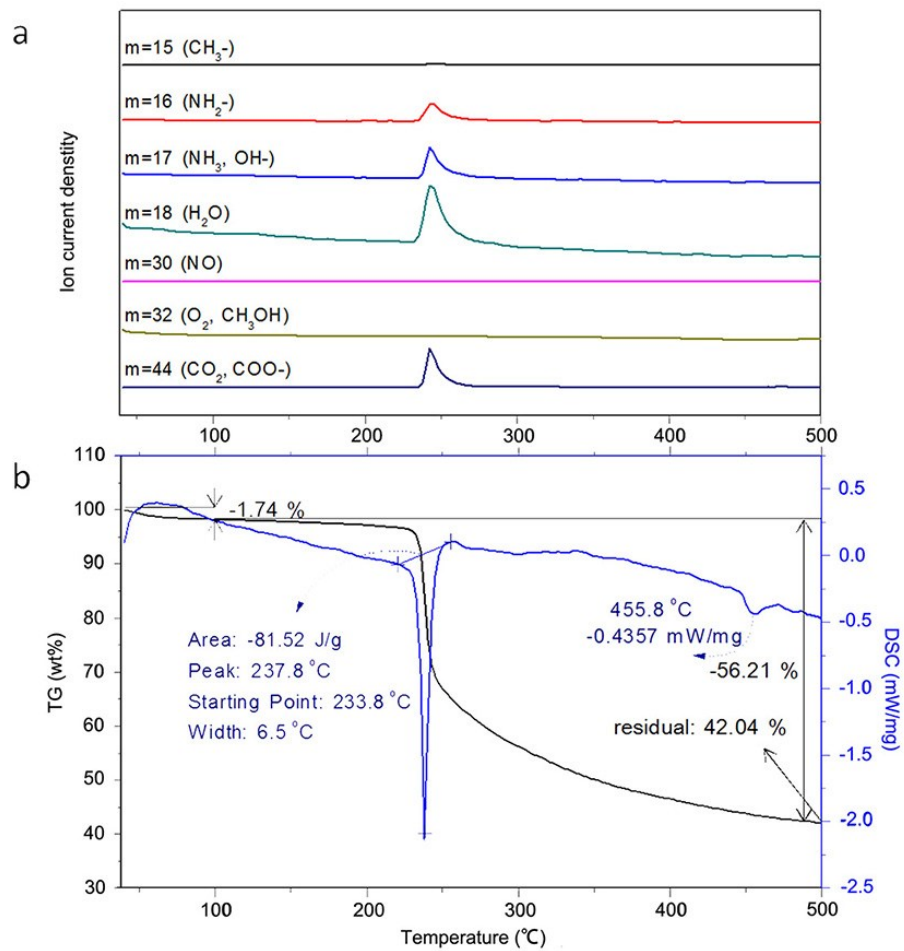


Fig. S8 TG-MS of **1** in Ar. a) Mass spectrum and b) TG-DSC.

TG-MS analysis in argon atmosphere was evacuated before heating. No chemical decomposition was observed before the peptide release temperature.

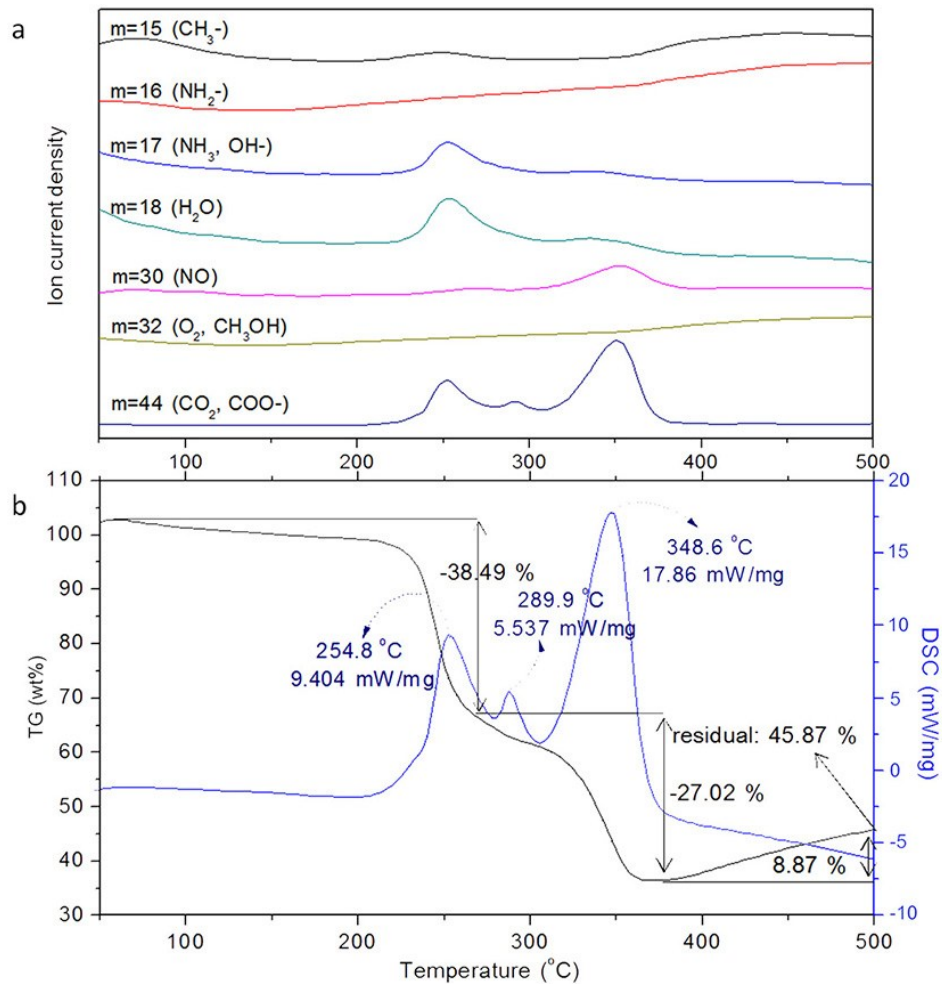


Fig. S9 TG-MS of **1** in air. a) Mass spectrum and b) TG-DSC.

TG-MS analysis in air was evacuated before heating and also indicates the thermal stability of the soft crystal in the atmosphere before 235 °C.

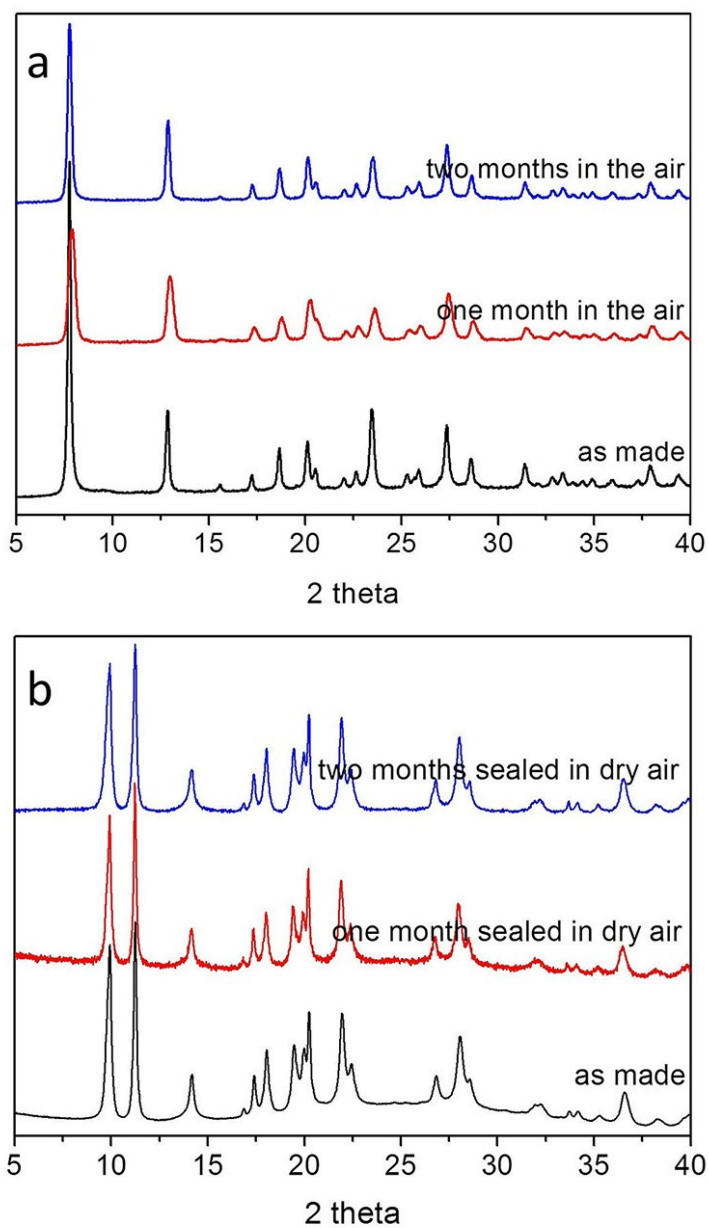


Fig. S10 XRD pattern of a) **1** and b) **1a** after storage under various conditions.

XRD confirmed the structural stability of **1** and **1a** when stored as solids at room temperature after two months.

4. Structure of **1b**

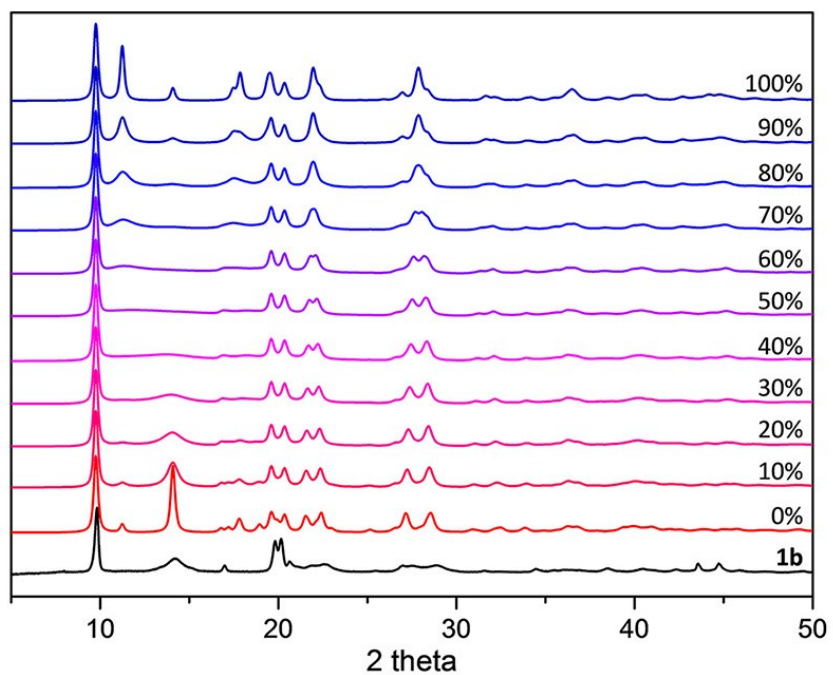


Fig. S11 Simulated PXRD by Diffax with different certain percentage of layer unflipped for the dry disordered sample. The X-shift and Y-shift are fixed at 0.4 and 0.5 respectively. (black: experimental data.)

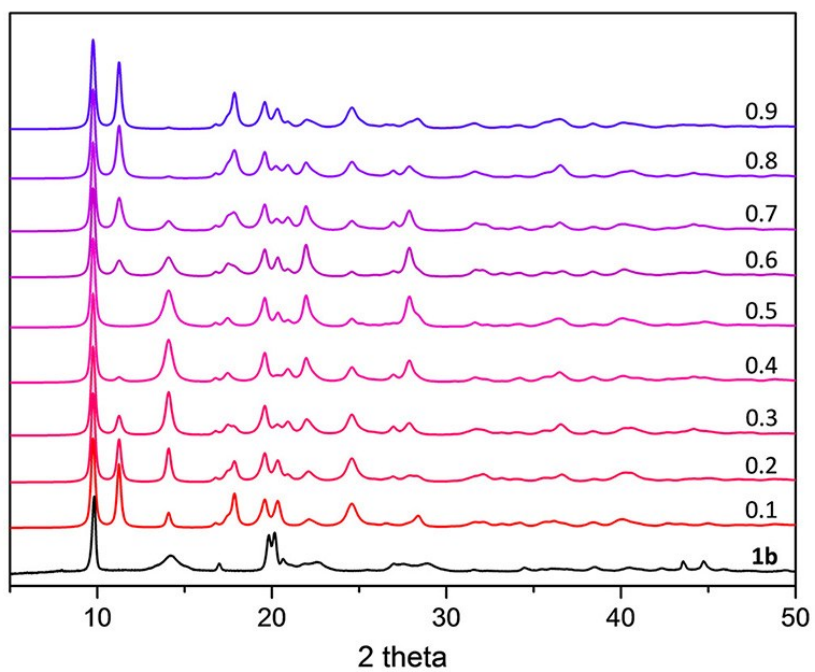


Fig. S12 Simulated PXRD by Diffax with different X-shift between adjacent layers for the dry disordered sample. The Y-shift is fixed at 0.5 with 20% layers unflipped. (black: experimental data.)

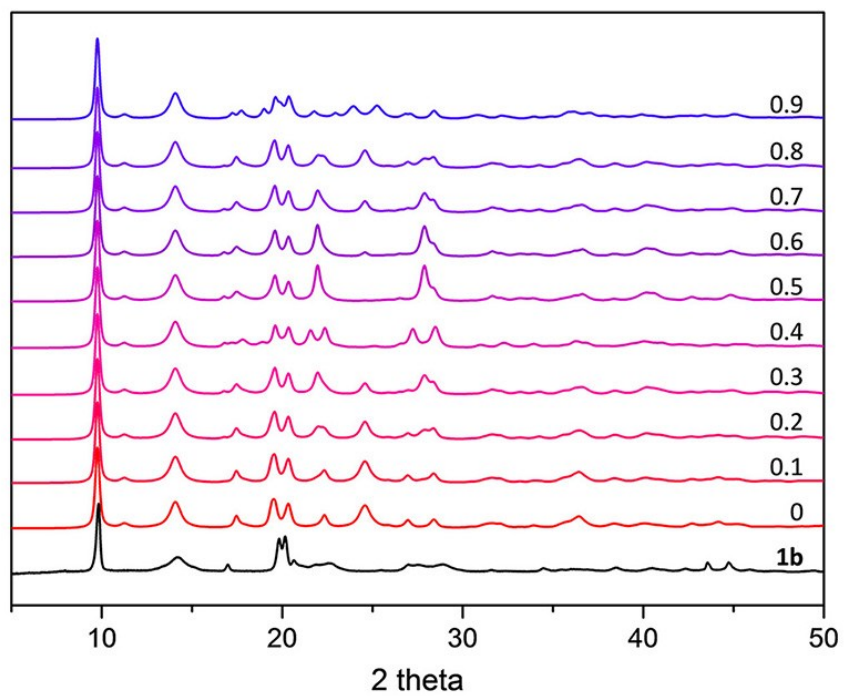


Fig. S13 Simulated PXRD by Diffax with different Y-shift between adjacent layers for the dry disordered sample. The X-shift is fixed at 0.4 with 20% layers unflipped. (black: experimental data.)

5. Thermal Stability Analysis of GT

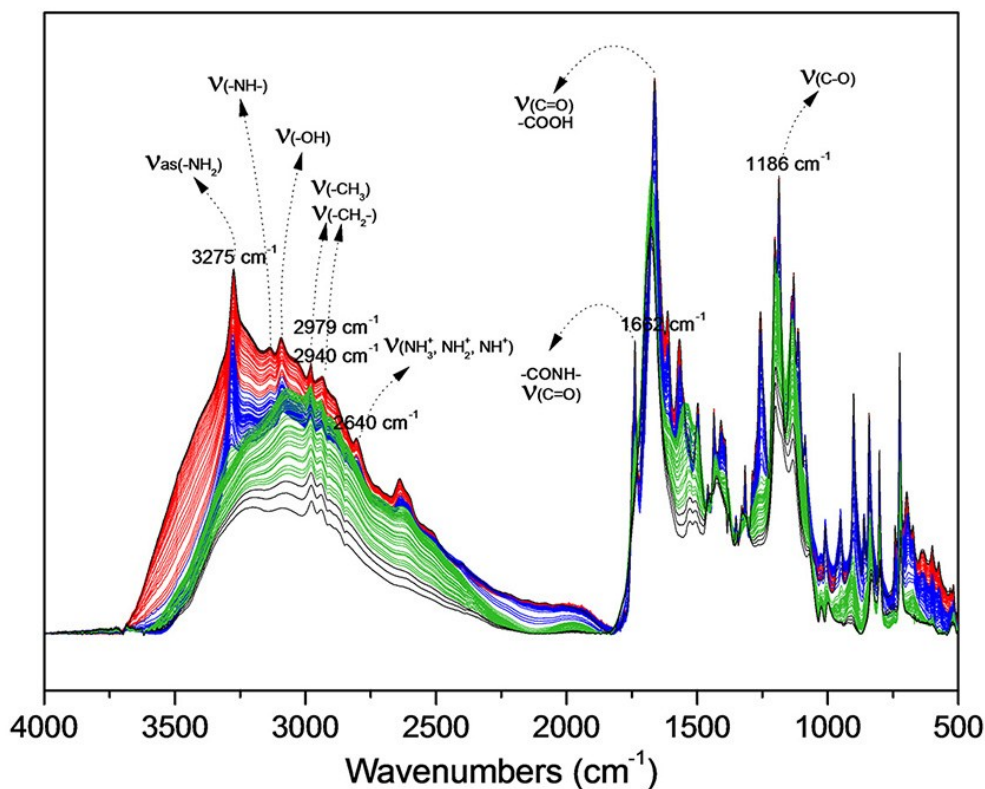


Fig. S14 *In situ* FT-IR of the peptide GT at the mentioned temperature ($^{\circ}\text{C}$) under air, from red to green represents temperatures from 25 $^{\circ}\text{C}$ to 220 $^{\circ}\text{C}$.

As shown in Fig. S14, both the $\nu(\text{N-H})$ bands at 3275 cm^{-1} and the $\nu(\text{C-OH})$ bands at 1250 cm^{-1} of carboxyl became blurred during heating of GT. Besides, the GT molecule was decomposed into fragments after being heated to 100 $^{\circ}\text{C}$, which was observed by mass spectrometry (Fig. S15), while the GT molecule in the crystal remains integrity after being heated (Fig. S16), indicating the high thermal stability of GT with ordered assembling.

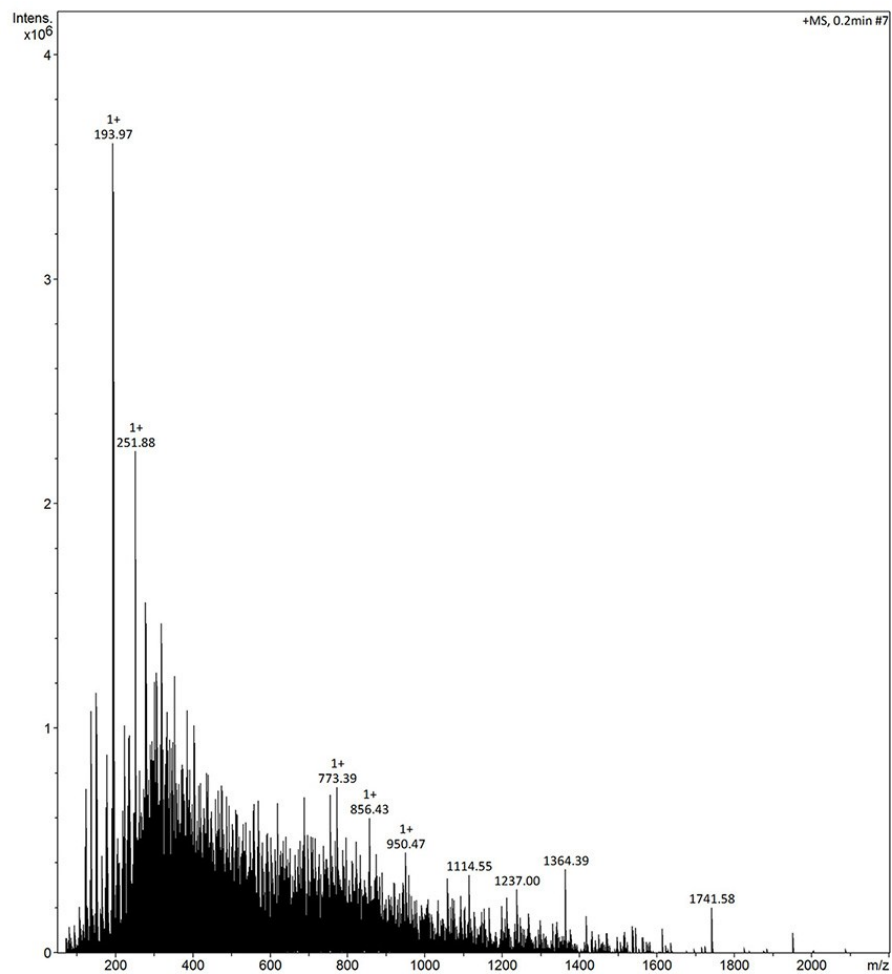


Fig. S15 Mass spectrum of GT after being heated to 100°C for 1 hour.

The structural information of GT after being heated shows the thermal instability of the dipeptide.

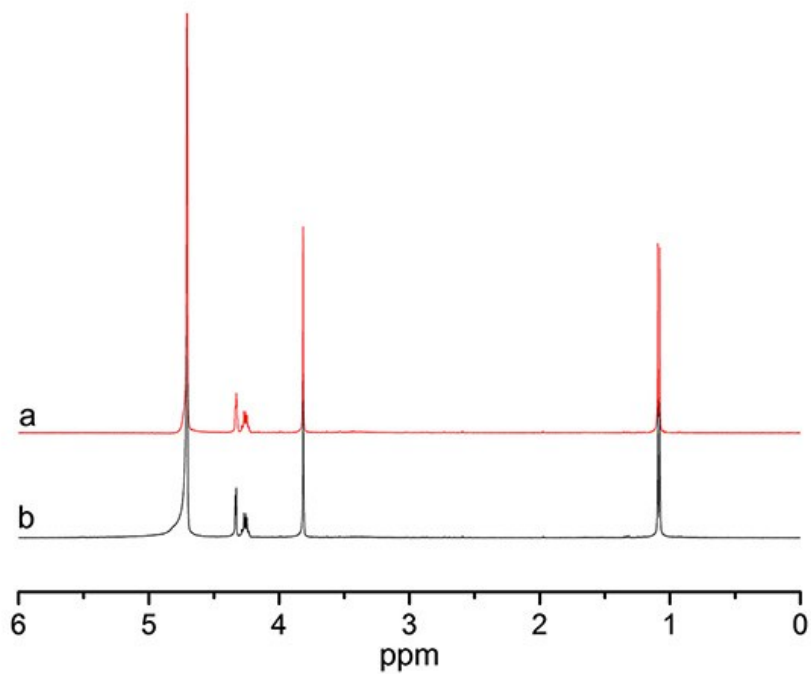


Fig. S16 a) ¹H NMR of **1** after being heated to 100°C and removed copper ions by neutral alumina column Chromatography. b) ¹H NMR of GT.

¹H NMR indicates the GT molecule in the crystal remains integrity after being heated to 100°C.

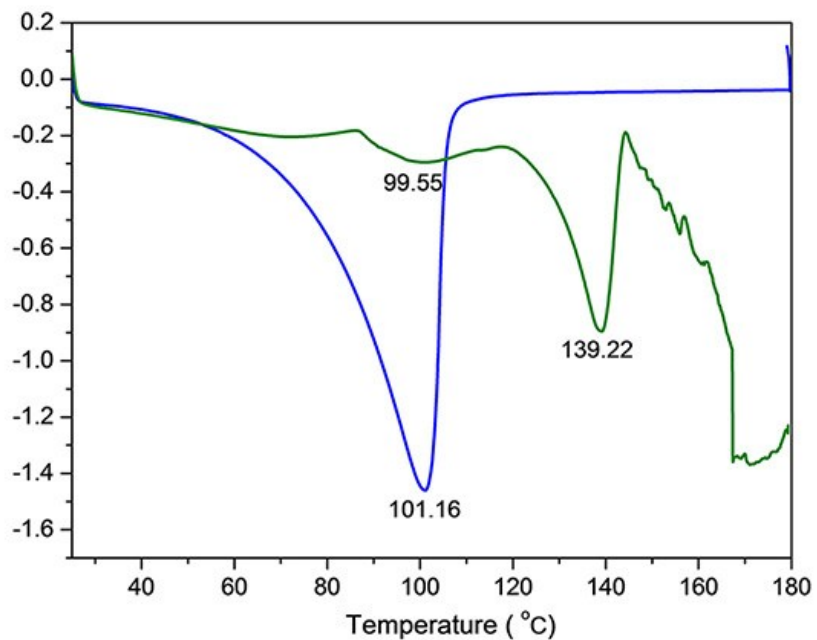


Fig. S17 Power-compensation DSC of **1** (blue) and GT (green).

DSC curve of **1** and GT in air confirmed the same exciting thermal stability of GT in the crystal of **1**. In other perspective, the result also indicates that GT molecular in **1** was not completely free from Cu^{2+} during the structural transformation.

6. Theoretical Calculation

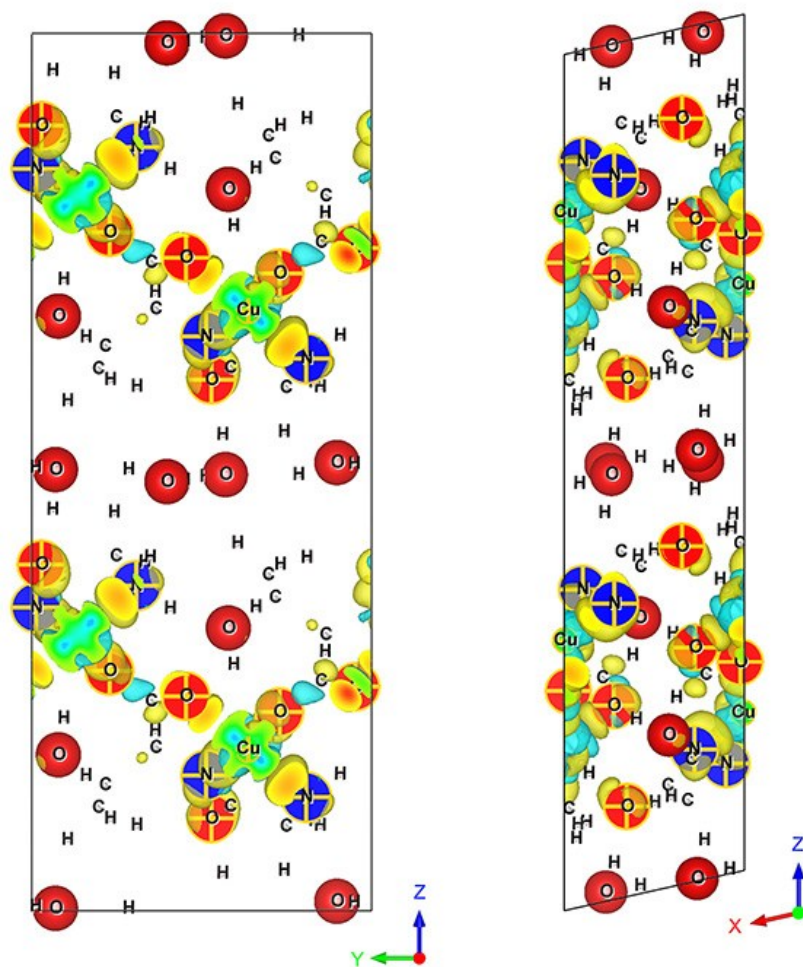


Fig. S18 Charge differential density distribution of **1** crystal structure whose separated parts are copper cation and ligands (upper panel). Cyan and yellow indicate depletion and accumulation charge respectively. The atoms were shown as ionic radii type balls.

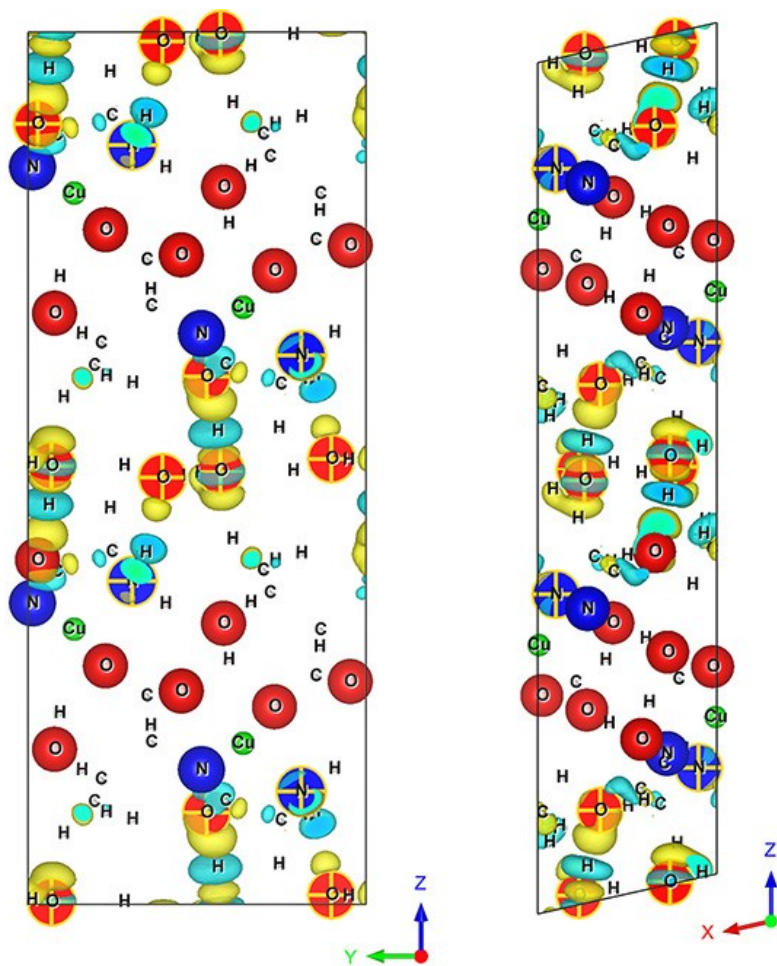


Fig. S19 Charge differential density distribution of that whose separated parts are water layers and structure of **1** without water layers (bottom panel). Cyan and yellow indicate depletion and accumulation charge, respectively. The atoms were shown as ionic radii type balls.

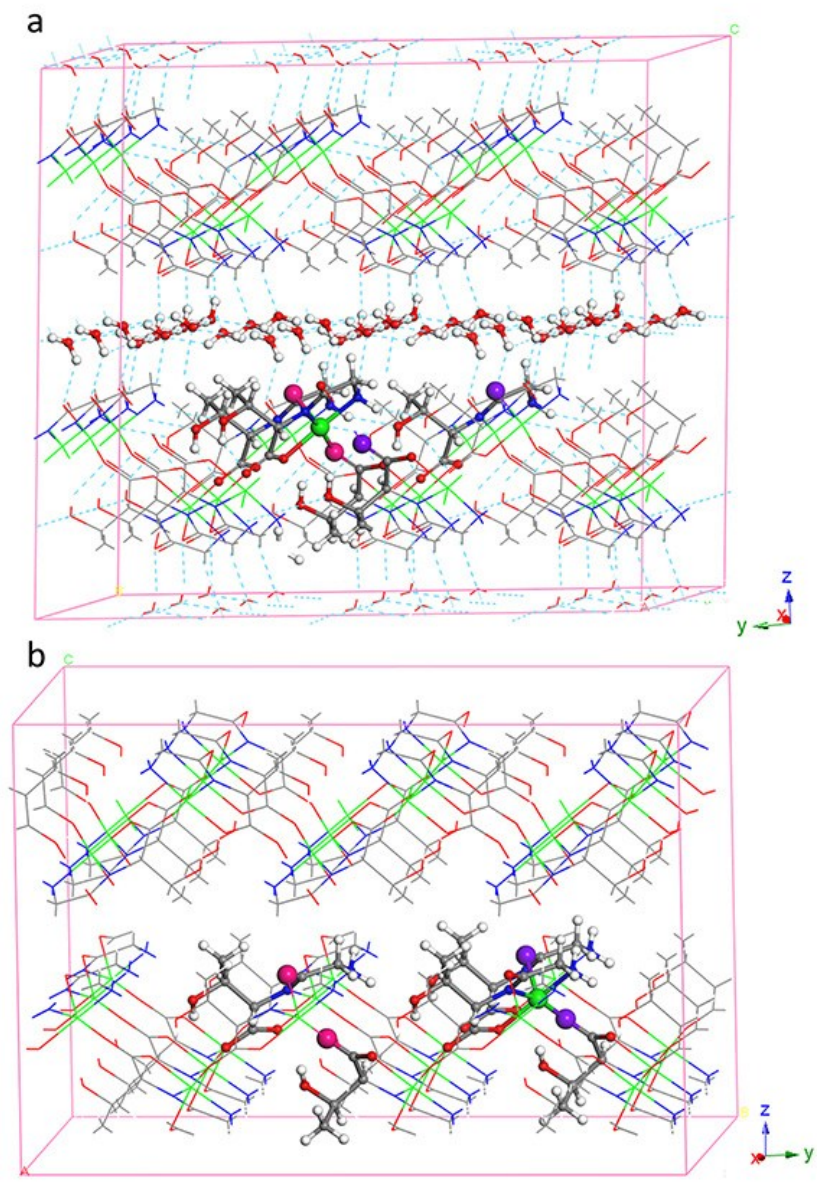


Fig. S20 Original models of (a) initial state and (b) final state. The green atoms stand for copper cations, and the rose red and purple atoms represent the initial and final oxygen atoms coordinated with copper cations, respectively.

7. Dynamic Adsorption

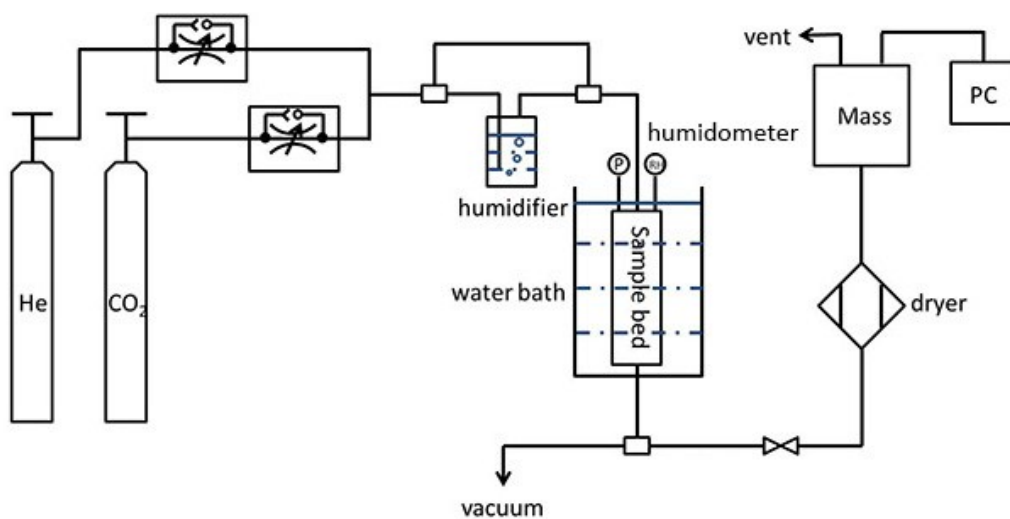


Fig. S21 Apparatus for the CO₂ breakthrough experiments under dry and wet conditions.

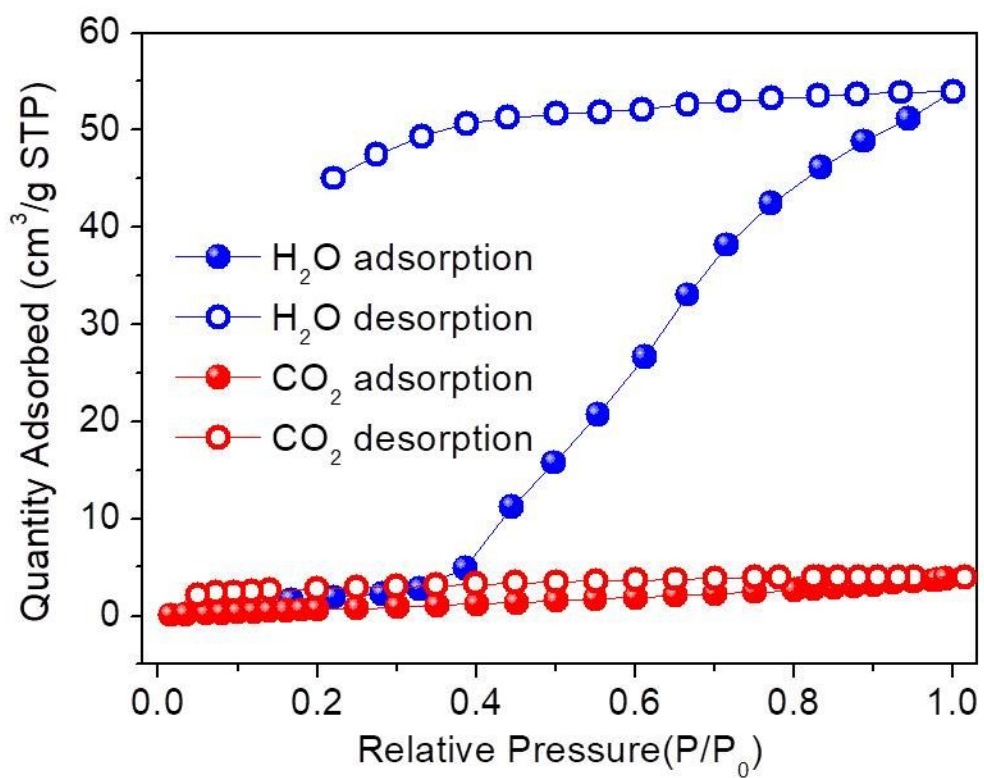


Fig. S22 H₂O and CO₂ sorption measurements.

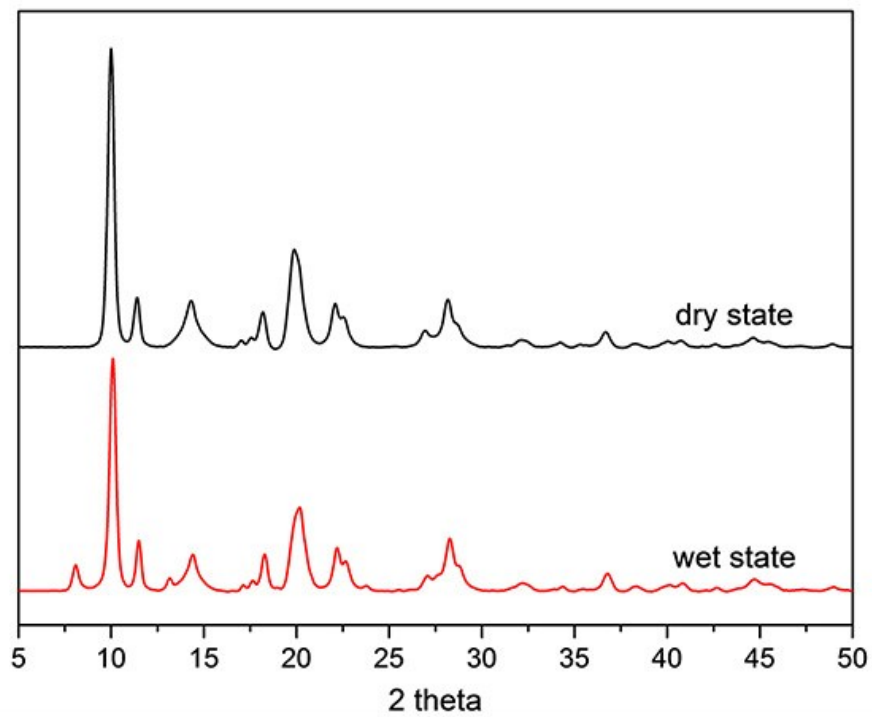


Fig. S23 PXRD patterns in the absence (dry state) or presence (wet state) of water.

Movie S1 & Movie S2. Movies for structural transformation from different perspectives.

References

- S1 G. M. Sheldrick. Program for solution of crystal structures, University of Göttingen, 1997.
- S2 O.V. Dolomanov, L.J. Bourhis, R.J. Gildea, J.A.K. Howard, H. Puschmann. *J. Appl. Crystallogr.* 2009, **42**, 339-341.
- S3 S. Grimme. *J. Comput. Chem.* 2006, **27**, 1787-1799.
- S4 C. Di Valentin. *J. Chem. Phys.* 2007, **127**, 154705-1-154705-8.
- S5 F. Labat, P. Baranek, C. Domain, C. Minot, C. Adamo. *J. Chem. Phys.* 2007, **126**, 154703-1-154703-12.
- S6 C. Di Valentin, E. Finazzi, G. Pacchioni, A. Selloni, S. Livraghi, A. M. Czoska, M. C. Paganini, E. Giamello. *Chem. Mater.* 2008, **20**, 3706-3714.
- S7 J. Hafner, *J. Comput. Chem.* 2008, **29**, 2044-2078.
- S8 N. D. Mermin. *Gas. Phys. Rev.* 1965, **137**, A1441-A1443.
- S9 P. E. Blöchl. *Phys. Rev. B.* 1994, **50**, 17953-17979.
- S10 G. Kresse, J. Joubert. *Phys. Rev. B.* 1999, **59**, 1758-1775.
- S11 J.P. Perdew. *Electronic Structure of Solids*, Akademie Verlag, Berlin, 1991, pp. 11-20.
- S12 R.M. Dreialer, E.K.U. Gross. *Density Functional Theory: An Approach to Quantum Many Body Problem*, Springer, Berlin, 1990, pp. 281-296.
- S13 B. Delley. *J. Chem. Phys.* 1990, **92**, 508-517.
- S14 B. Delley. *J. Chem. Phys.* 2000, **113**, 7756-7764.